Dual-curve-fitting-based Wind Parameter Extraction from Shipborne Nautical X-Band Radar Data

Ying Liu, *Student Member, IEEE,* Weimin Huang, *Senior Member, IEEE,*
Eric W. Gill, *Senior Member, IEEE,* Dennis K. Peters, *Senior Member, IEEE,*
Faculty of Engineering and Applied Science, Memorial University of Newfoundland
St. John's, NF, Canada, A1B 3X5

***Abstract*—In this paper, techniques for retrieving wind direction and speed from shipborne X-band nautical radar images are presented. First, by analyzing the radar backscatter intensity histogram and zero-pixel percentage, each individual image is designed to go through a data quality control process. With this processing, the rain cases and all-black images can be recognized. Then, a harmonic function that is least-squares fitted to the radar backscatter intensity as a function of antenna look direction is applied to determine the wind direction. Furthermore, for wind speed retrieval, an empirical third-order polynomial model is derived using the average radar backscatter intensity and the reference wind speed. To improve the accuracy of wind retrieval, a modified technique, which involves a dual-curve-fitting approach, is implemented. For the data presented in this paper, it was found that the second stage of the curve-fitting performed optimally when the data at angles of 60° to the left and right of the first-guess upwind direction were used. Also, only the data for the dual-curve-fitting were used to calculate the average intensity of the radar images for wind speed estimation. The modified method is applied to the radar data and the results are compared with the reference data measured by a ship-based anemometer. It is shown that the dual-curve-fitting algorithm produces improvements in the mean differences between the radar and the anemometer results for wind direction and speed of about 7° and 0.4 m/s, respectively, under low sea state.**

***Index Terms*—Shipborne, wind retrieval, X-band, nautical radar.**

I. Introduction

Wind information is important for studying the energy exchange processes between the atmosphere and the ocean surface. The most common wind measurement tools are cup or ultrasonic anemometers. However, ship-mounted anemometer measurements may be negatively impacted by effects which the hull and superstructure have on the air flow to the instrument (air flow distortion) [1]. This is one of the main reasons why attempts are now being made to retrieve wind information from nautical radar images. Moreover, compared to traditional *in-situ* measurements, radar-based sea surface wind measurements have an additional advantage that they are independent of the sensor's height and motion [2].

Among the work related to the extraction of wind information from nautical radar images, the algorithms proposed by Dankert *et al* [3], Lund *et al* [1], and Vicen-Bueno *et al* [4] have been effectively implemented. Dankert *et al* [3] determine the wind direction from quasi-stationary wind streaks and derive wind speed from the temporally integrated radar images and the estimated wind direction. However, this approach cannot be directly applied to shipborne radar data, because wind streaks are difficult to extract due to the platform's horizontal motion, and a 180° directional ambiguity exists in the wind direction results [2].

To overcome previously existing limitations, both Lund *et al* [1] and Vicen-Bueno *et al* [4] developed methods which are independent of platform movement. By utilizing the radar backscatter intensity dependence on the upwind direction, Lund *et al* [1] proposed an least-squares fit technique to identify the upwind peak in the range-averaged backscatter as a function of the antenna look direction. To obtain wind speed , an empirical third-order polynomial is derived using the mean radar backscatter intensity and the reference wind speed. Vicen-Bueno *et al* [4] proposed an effective backscatter intensity level selection algorithm based on temporal integration and smoothing to extract wind direction, and the wind speed was retrieved from an empirical third-order polynomial geophysical model function (GMF).

In this paper, the data in the directions due to blockage were excluded, and the algorithm of Lund *et al* is applied to the shipborne radar data since the curve-fitting technique works well even if some sections of the radar field of view are masked [1]. However, for some images, in many azimuthal directions a majority of the pixels may have a very low intensity. These dark regions are not due to the obstruction by ship structures but probably result from low sea states. These low-intensity data are retained in the curve-fitting process. Unfortunately, in these low-intensity azimuthal directions, the fitted curve is not satisfactory. Under these circumstances, a dual-curve-fitting was implemented to reduce the wind estimation error.

This paper is organized as follows. In Section II, the curve-fitting-based wind retrieval algorithms are introduced and some modifications are proposed. In Section III, the X-band radar data and the reference wind data are described. Section IV introduces the data quality control procedures, including the recognition of rain and black-images. The results of wind direction and speed determination are discussed in Section V. Finally, Section VI contains a summary and reiterates the main conclusion of this work.

II. Wind Retrieval Algorithm

In this section, the algorithms for determining wind direction and speed are introduced. A cosine function that is

978-1-4799-3646-5/14/$31.00 ©2014 IEEE

least-squares fitted to the radar backscatter intensity is used to ascertain the wind direction (i.e., single-curve-fitting). Then, a modified dual-curve-fitting approach is proposed to improve the accuracy of wind retrieval. Moreover, an empirical third-order polynomial model is constructed to determine wind speed from the calculated average intensity value.

A. Wind Direction

1) Single-Curve-Fitting: It is known that nautical X-band radar backscatter received from the ocean is modulated by the small-scale surface roughness (3 cm) due to Bragg scattering. For HH-polarized X-band radars operating at grazing incidence, the radar backscatter dependency on antenna look direction has been observed. The backscatter intensity has a single peak in the upwind direction, and a second peak appears in downwind direction [5] [6]. To obtain the radar backscatter dependency on range and antenna look direction, radar pulses are averaged over range and are then curve fitted [1]. A cosine square function

$$\sigma_\theta = a_0 + a_1 \cos^2(0.5(\theta - a_2)) \qquad (1)$$

is least-squares fitted to the radar data (blue line). Here σ_θ is the range-averaged radar backscatter intensity as a function of antenna look direction θ. a_0, a_1, and a_2 are the regression parameters. An example of curve-fitting is shown in Fig. 1. The best-fit curve is shown in red. For each individual radar image, the wind direction can be retrieved from the upwind backscatter peak by using the model-function, Eq. (1). The upwind peak direction is given by the regression parameter a_2. This corresponds to the peak of the best-fit curve, as discussed in [1].

2) Dual-Curve-Fitting: To retrieve wind direction from a single image, the radar backscatter intensities from the non-obstructed antenna look directions are averaged over range to perform the curve-fitting. It is assumed that this functions well even if some sections of the radar field of view are masked. In our data collection, the data in the directions due to blockage were excluded. However, for some images in many azimuthal directions, a majority of the pixels may have a very low intensity. These dark regions are not due to the obstruction by ship structures but probably result from low sea states. These low-intensity data are retained in the curve-fitting process. Unfortunately, as shown in Fig. 2(b), in these low-intensity azimuthal directions, the single-curve-fitting result is not ideal. In this case, a dual-curve-fitting was implemented. The technique involves using the data at angles of 60° to the left and right of the first-guess upwind direction to perform the curve-fitting again, as shown in Fig. 2(c). This

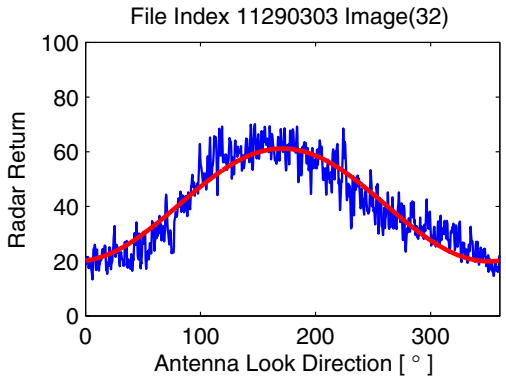

Fig. 1. Range-averaged radar backscatter intensity as a function of antenna look direction for image collected at 03:03 UTC, November 29.

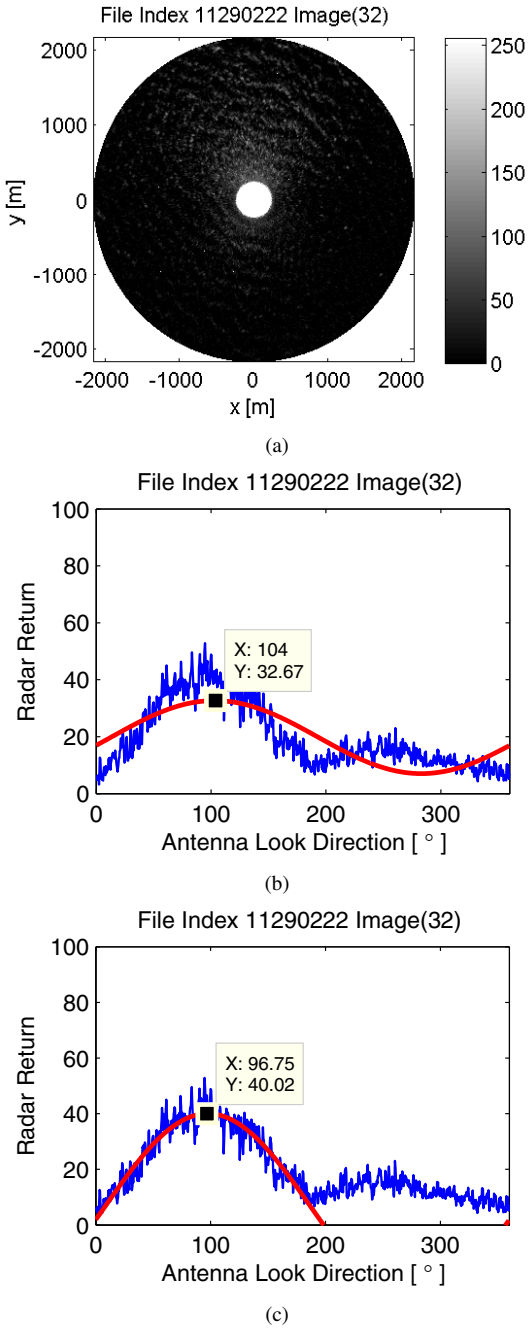

Fig. 2. a) Radar backscatter image. b) Range-averaged radar backscatter intensity as a function of antenna look direction using single-curve-fitting. c) Range averaged radar backscatter intensity as a function of antenna look direction using dual-curve-fitting. (Data collected at 02:22 UTC, November 29.)

dual-curve-fitting results in an improvement of about 7° in this example, as compared to that obtained using a single-curve-fitting.

B. Wind Speed

Based on the radar backscatter intensity dependence on wind speed, an empirical third-order polynomial can be derived using the average radar backscatter intensity and the reference wind speed. Then, radar wind speed results can be retrieved from the average intensity value. The average radar backscatter intensity is calculated as [1]

$$\sigma_{wSpd} = \frac{1}{2\pi}\int_0^{2\pi}(a_0 + a_1\cos^2(0.5(\theta - a_2)))d\theta, \quad (2)$$

It should be noted that the data in the obstructed directions are excluded. Also, when the dual-curve-fitting is applied, only the data at angles of 60° to the left and right of the first-guess upwind direction are used to evaluate the average radar backscatter intensity. Fig. 3 shows a scatter plot of the anemometer-measured wind speed and the corresponding radar average backscatter intensities σ_{wSpd}. The red curve is derived using a least-squares method based on a third-degree polynomial function as in [1].

III. Data Overview

The data used for testing were provided by Defence Research and Development Canada (DRDC). The marine radar utilized in the experiment is a standard shipborne nautical radar (Decca BridgeMaster II 340), which operates at 9.5 GHz. The antenna rotation period (the time for one radar image) is about 2 s. The radar covers 360° in azimuth, but blockage due to ship's structure may result in dark regions in some images. Each image has an approximate azimuthal resolution of 0.4°. The radar range extends to 2160 m (starting at 240 m in the near range) with a range resolution of 7.5 m. The marine radar was connected to an analog-to-digital (AD) converter. This AD converter was incorporated in the Wave Monitoring System II (WaMoS II) [7]. The system digitizes the radar backscatter intensities by azimuth-range bin and scales data into 8-bit unsigned integers ([0, 255]). Every 32 images are combined into one file, and the file index reveals the start time of each file.

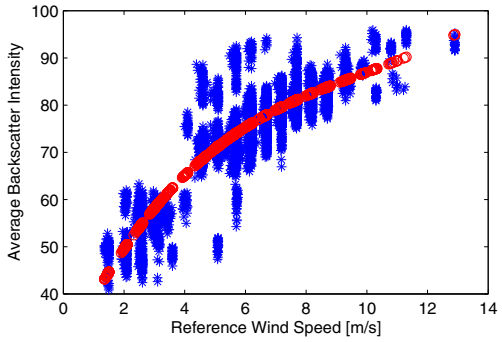

Fig. 3. Scatter plot showing the wind speed from anemometer, corresponding radar backscatter intensity, and the best-fit curve based on a third-degree polynomial function for data acquired during November 29∼30, 2008.

The shipborne anemometer and marine radar data were collected approximately 150 miles from the coast of Halifax (42° N, 62° W) in late November, 2008. The anemometer wind data were affected by the ship's motion. Thus, the reference wind speed and direction must be corrected by removing the ship's motion.

IV. Quality Control

Before using the radar data to determine the upwind direction and wind speed, a data quality control procedure was undertaken for each image by analyzing the radar backscatter intensity histogram and zero-pixel percentage. The procedure includes the recognition of rain and all-black images. Examples of the corresponding radar backscatter image and its histogram can be found in [8].

A. Rain Recognition

It was found that X-band radar backscatter intensity will be enhanced by the rain effects on the sea surface and the rain-related wind effects [9]. According to [1], due to the strong impact of rain on the number of pixels with zero intensity, the zero-pixel percentage (i.e., ratio, expressed as a percentage, of the number of image pixels with zero intensity to the overall number of pixels) was identified as a quality control parameter to determine the presence of rain. For the data presented in this paper, pixels with intensities lower than 5 were considered as zero-intensity. The overall percentage of pixels with intensities from 0 to 5 was defined as zero-pixel percentage. When the zero-pixel percentage of the image was below 10%, the image was regarded as contaminated by rain, and it was excluded from wind retrieval.

B. All-Black Image Recognition

As a result of a large noise content or unknown system errors, some images may appear black with little wave signature. These images are referred to black-images. In this paper, an image with a zero-pixel percentage above 60% is flagged as a black-image and is excluded from the wind algorithm.

V. Recovery of Wind Parameters

The modified method described above was applied to the quality-controlled radar data and the results were referenced to data measured by a ship-based anemometer (with the ship's motion removed). It should be noted that the GPS records the ship direction relative to true north while the anemometer output is with respect to magnetic north. The magnetic declination compensation was implemented to correct the reference wind speed and direction relative to true north. Using the tools provided by Natural Resources Canada [10], the magnetic declination (Date: 2008-11-29, Latitude: 42° North, Longitude: 61° West) was shown to be approximately 18°.

Fig. 4 shows the comparison of the radar-derived wind velocities using single- and dual-curve-fitting methods with

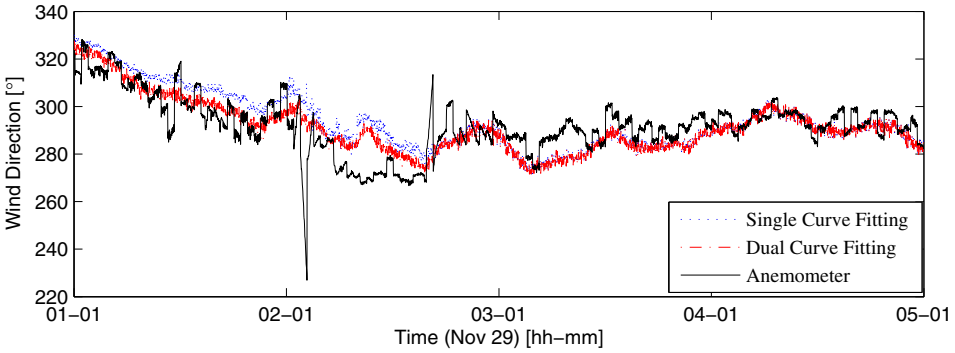

(a)

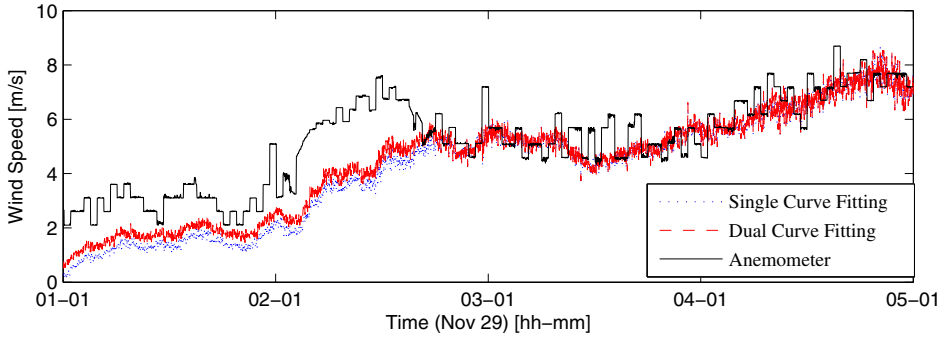

(b)

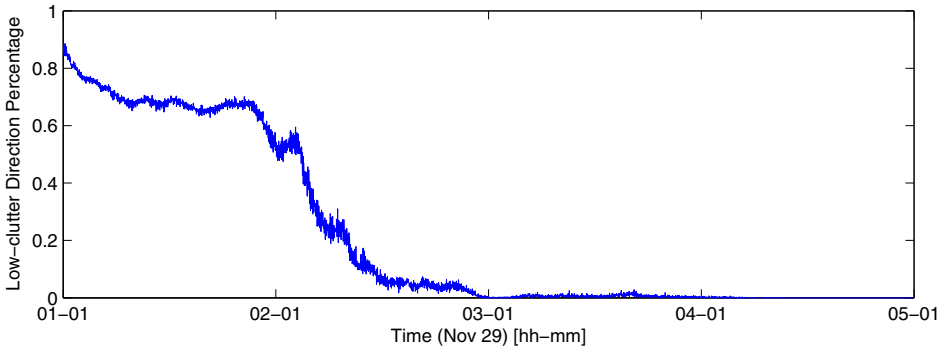

(c)

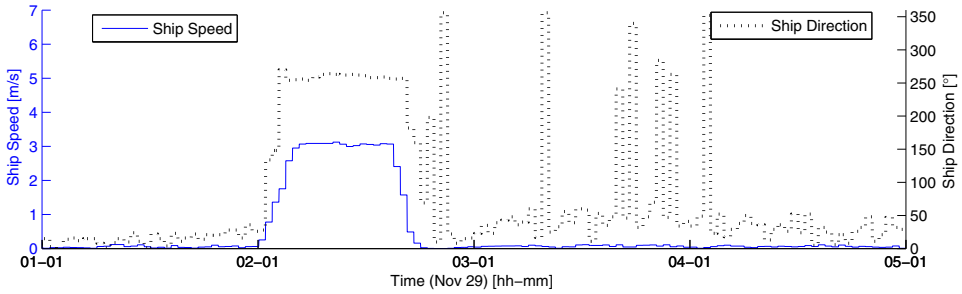

(d)

Fig. 4. Comparison of wind results from 01:00 UTC to 05:01 UTC, November 29, 2008. a) Wind direction; b) Wind speed; c) Percentage of directions with many low intensity pixels; d) Ship speed and ship direction.

the anemometer-measured results based on the data collected during 01:00 UTC to 05:01 UTC, November 29. It can be seen that the radar results from both methods agree well with the anemometer data. However, improvement using dual-curve-fitting is seen during 01:00 to 02:10, as shown in Fig. 4(a). During this period, the wind speed is lower than 4 m/s and the percentage of directions with many low intensity pixels is above 50% based on the low-clutter direction percentage analysis (see Fig. 4(c)). Taking the anemometer results as the ground truth, the mean errors of wind direction and speed using single-curve-fitting are found to be 11.3° and 1.89 m/s, respectively, and those for dual-curve-fitting are, respectively, 4.30° and 1.49 m/s. Thus, the results indicate that the mean errors of wind direction may be improved by about 7° during low sea states. The performances of the single- and dual-curve-fitting techniques are almost the same when the wind speed is higher than 4 m/s, under which condition the clutter is strong in almost all azimuthal directions (see Fig. 4(b) and 4(c)).

VI. Conclusion

In this paper, algorithms for wind retrieval from shipborne X-band nautical radar images were investigated. First, a data quality control process was performed for each image, including the recognition of rain and all-black images. Then, based on Lund's method [8], a least-squares curve-fitting technique was applied to determine the wind direction, and a dual-curve-fitting approach was implemented to improve the accuracy of wind direction. Finally, for wind speed retrieval, only the data for the dual-curve-fitting were used to obtain the average intensity of the radar images. It is seen that the mean difference bwteen the radar and anemometer results for wind direction can be improved by about 7° under low sea state periods.

A couple of limitations of the method should be noted: Firstly, the empirical polynomial model may be influenced by rain. For each individual radar system, the threshold of the zero-pixel percentage as a data quality control parameter for rain recognition may differ greatly. In Lund's work, the threshold was 50% while our value was set to 10%. This is due to the differences in the digitalization level of the radar backscatter intensity. Also, some datasets show that rain recognition was not successful. A more robust way to identify rain cases is required. Secondly, although the data quality control works well, our results show that when the ship's motion changes significantly, the empirical polynomial model for wind speed will be affected. In order to improve the robustness of the model, it is suggested to use the data with low ship speed to train the model and to test the data without the low ship speed restriction.

Acknowledgment

This work was supported by Natural Sciences and Engineering Research Council of Canada grants to Dr. E. W. Gill (NSERC 238263-10) and Dr. W. Huang (NSERC 402313-12), an Atlantic Innovation Fund (AIF) to Dr. E. W. Gill, and an Research and Development Corporation (RDC) IRIF Ignite grant (207765) to Dr. W. Huang. The authors would also like to thank Dr. E. Thornhill of Defence Research and Development Canada (DRDC) for providing the radar and buoy data.

References

[1] B. Lund, H. C. Graber, and R. Romeiser, "Wind retrieval from shipborne nautical X-band radar data," *IEEE. Trans. Geosci. Rem. Sens.*, vol. 50, pp. 3800-3811, 2012.

[2] B. Lund, "Development and evaluation of new algorithms for the retrieval of wind and internal wave parameters from shipborne marine radar data," *PhD thesis, University of Miami, Rosenstiel School of Marine and Atmospheric Science,* 2012.

[3] H. Dankert, J. Horstmann, and W. Rosenthal, "Ocean wind fields retrieved from radar-image sequences," *J. Geophys. Res.: Oceans (1878-2012)*, no. C11, 2003.

[4] R. V. Bueno, J. Horstmann, E. Terril, T. D. Paolo, and J. Dannenberg, "Real-Time Ocean Wind Vector Retrieval from Marine Radar Image Sequences Acquired at Grazing Angle," *J. Atmos. Oceanic Technol.*, vol. 30, pp.127-139, 2013.

[5] H. Hatten, J. Seemann, J. Horstmann, and F. Ziemer, "Azimuthal dependence of the radar cross section and the spectral background noise of a nautical radar at grazing incidence," *Proc. Geosci. Rem. Sens. Symp.*, vol. 5, pp. 2490-2492, 1998.

[6] W. J. Plant, "A two-scale model of short wind-generated waves and scatterometry," *J. Geophys. Res.*, vol. 91, pp. 10735-10759, 1986.

[7] "WaMoS II Wave and surface current monitoring system operating manual version 4.0." (2012, May) [Online]. Available: oceanwaves.org

[8] Y. Liu, W. Huang, E. W. Gill, and D. Peters, "Wind direction retrieval from shipborne nautical X-band radar data," *IEEE NECEC Conference*, Newfoundland, Canada, 2013.

[9] W. Alpers, C. Melsheimer. (2013, Jun.) "SAR marine users manual-Chapter 17- Rainfall." [Online]. Available: sarusersmanual.com

[10] "Magnetic declination calculator." (2013, Jun.) *Natural Resources Canada.* [Online]. Available: geomag.nrcan.gc.ca